Finger-Shaped GelForce: Sensor for Measuring Surface Traction Fields for Robotic Hand

Katsunari Sato, *Student Member*, *IEEE*, Kazuto Kamiyama, Naoki Kawakami, and Susumu Tachi, *Member*, *IEEE*

Abstract—It is believed that the use of haptic sensors to measure the magnitude, direction, and distribution of a force will enable a robotic hand to perform dexterous operations. Therefore, we develop a new type of finger-shaped haptic sensor using GelForce technology. GelForce is a vision-based sensor that can be used to measure the distribution of force vectors, or surface traction fields. The simple structure of the GelForce enables us to develop a compact finger-shaped GelForce for the robotic hand. GelForce that is developed on the basis of an elastic theory can be used to calculate surface traction fields using a conversion equation. However, this conversion equation cannot be analytically solved when the elastic body of the sensor has a complicated shape such as the shape of a finger. Therefore, we propose an observational method and construct a prototype of the finger-shaped GelForce. By using this prototype, we evaluate the basic performance of the finger-shaped GelForce. Then, we conduct a field test by performing grasping operations using a robotic hand. The results of this test show that using the observational method, the finger-shaped GelForce can be successfully used in a robotic hand.

Index Terms—Force sensor, surface traction field, finger shape, robotic hand.

1 Introduction

Humanoid robots are made to adapt to the environment in which human beings live and assist humans in their daily life. Human beings have longed for such robots found in science fiction and tried to realize them. In recent years, there has been a remarkable development in humanoid robots; in addition, robots that are capable of assisting patients or doing housework instead of human beings have been developed. Haptic information acquired by a sensor is important in enabling these robots to perform dexterous operations. In particular, a haptic sensor for a robotic finger is considered to be an important device because the finger of a humanoid robot is the most useful part of its body when it is used to manipulate an object. These robots can stably grasp an object using their hands on the basis of haptic information such as reflective force, frictional force, and point of contact with the object. Therefore, a number of haptic sensors for use in robotic hands have been developed [1], [2].

The objective of this study is to develop a finger-shaped haptic sensor for a humanoid robot (Fig. 1). While developing such haptic sensor for a robotic finger, we should take into consideration its requirements. These requirements are described as follows: First, the sensor should be able to measure the magnitude, direction, and distribution of an applied force or a *surface traction field*. Human beings perceive all three parameters and grasp an object safely and dexterously, even if the object is fragile. Similarly, robots must be able to detect surface traction fields. Second, the size of the sensor should be small. In order to integrate many haptic sensors in a humanoid robot hand, it is preferable to use compact sensors. Finally, the sensor should be a high-performance device. In order to use this sensor in our daily life, we need to ensure that the magnitude, spatial, and temporal sensing performance are the same as those perceived by human beings. For example, human begins can detect approximately 0.5 mN force applied to the skin [3], distinguish two applied forces separating approximately 1.2-1.7 mm [4], and perceive vibration up to 700 Hz [5].

Nearly all existing haptic sensors for robotic hands [6], [7], [8] belong to one of the following two categories. Sensors that belong to the first category are used to measure a force vector at a single point; we call them *force vector sensors*. Sensors that belong to the second category are used to measure the distribution of forces; however, these sensors can only measure the magnitude of a force and not its direction. We call such sensors as *force distribution sensors*. These sensors are employed with a sensing unit, where mechanical pressure is exerted. Therefore, sensors that can be used to measure surface traction fields can be developed by integrating many force vector sensor elements. However, it is difficult to realize a sensor with small size and high resolution, because the use of many sensors can complicate the sensor structure.

Another approach to measure the surface traction fields involves the use of optics [9], [10], [11], [12]. However, it is still difficult to satisfy all the abovementioned requirements using optics. For example, Ferrier and Brockett [10] have

- *K. Sato and N. Kawakami are with the Graduate School of Information Science and Technology, The University of Tokyo, 7-3-1 Hongo, Bunkyo-ku, Tokyo 113-8656, Japan. E-mail: {Katsunari_Sato, Naoki_Kawakami}@ipc.i.u-tokyo.ac.jp.*
- *K. Kamiyama is with the Department of Human Communication, The University of Electro Communications, 1-5-1 Chohugaoka, Chohu-city, Tokyo 182-8585, Japan. E-mail: kamiyama@hc.uec.ac.jp.*
- *S. Tachi is with the Graduate School of Media Design, Keio University, 4-1-1 Hiyoshi, Kohoku-ku, Yokohama City, Kanagawa 223-8526, Japan. E-mail: tachi@tachilab.org.*

Manuscript received 15 Nov. 2008; revised 30 July 2009; accepted 24 Sept. 2009; published online 22 Oct. 2009
Recommended for acceptance by Y. Yokokohji.
For information on obtaining reprints of this article, please send e-mail to: toh@computer.org, and reference IEEECS Log Number THSI-2008-11-0088.
Digital Object Identifier no. 10.1109/ToH.2009.47.

Fig. 1. Example of operation performed by a robotic hand using our finger-shaped sensor. The top and bottom surfaces shown on the laptop display represent surface traction field measured by the sensors mounted on the index finger and the thumb of the robotic hand, respectively.

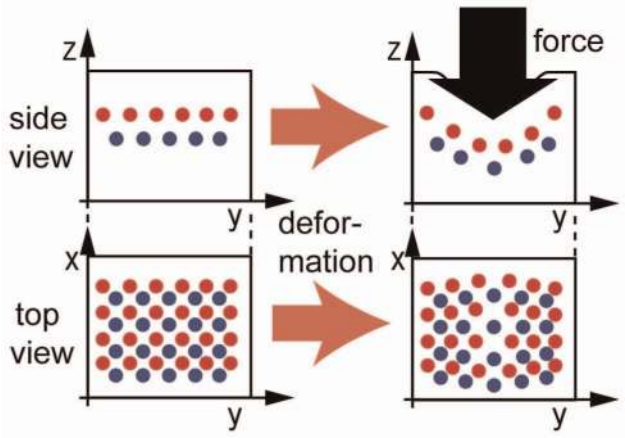

Fig. 2. Movements of markers in the elastic sensor body caused by force applied to the sensor surface [12].

developed a small tactile sensor that can be used to track dots on an elastic material in order to compute the 3D configuration of a finger-shaped elastic membrane. Unfortunately, a complex processing method is required for this sensor to acquire the direction of force, which could potentially lead to inaccuracy and instability of calculation of the surface traction fields. In addition, Kamiyama et al. [12] have developed a GelForce that is based on an elastic theory. GelForce has a simple structure; therefore, it satisfies the second and third requirements, i.e., it is small in size, and it has high resolution. However, the elastic theory is applicable to a semi-infinite elastic body. Therefore, the surface of a conventional GelForce is a plane.

In this study, in order to satisfy all the above mentioned requirements, we develop a finger-shaped haptic sensor using GelForce technology. Because of the complicated shape of a finger, the elastic theory cannot be analytically resolved by the finger-shaped GelForce. Therefore, we propose an observational method to calculate surface traction fields using the finger-shaped GelForce. In this paper, we present the principle, design, and observational method of the finger-shaped GelForce. Then, we present the result of an evaluation of a prototype finger-shaped GelForce to confirm 1) that proposed method is applicable and 2) that the finger-shaped GelForce can be applied to operations conducted by a robotic hand. We compared the basic performance of the finger-shaped GelForce with that of the conventional GelForce. We also conducted a field test on the finger-shaped GelForce using a robotic hand.

2 Finger-Shaped GelForce

2.1 Basic Principle of GelForce

We developed a finger-shaped sensor using the same technology used to develop GelForce [12]. This sensor consists of a transparent elastic body, light (red) and dark (blue) gray marker matrixes, and a color charge-coupled device (CCD) camera that captures the movements of the markers. When a force is applied to the surface, the markers move in response to the magnitude and direction of the force (Fig. 2). The movements of the markers are captured by the camera. We calculate the center of the markers before and after the application of the force to calculate the movements. When we assume that the deformation of the elastic body is linear, the relationship between the two-dimensional movements of m-markers u and the three-dimensional n-force vectors f is given by using conversion matrix H.

$$u = Hf.$$

$$u = \begin{bmatrix} u_{Rx} \\ u_{Ry} \\ u_{Bx} \\ u_{By} \end{bmatrix}, \quad H = \begin{bmatrix} h_{Rxx}, h_{Ryx}, h_{Rzx} \\ h_{Rxy}, h_{Ryy}, h_{Rzy} \\ h_{Bxx}, h_{Byx}, h_{Bzx} \\ h_{Bxy}, h_{Byy}, h_{Bzy} \end{bmatrix}, \quad f = \begin{bmatrix} f_x \\ f_y \\ f_z \end{bmatrix}. \quad (1)$$

In this equation, u_{Rp}, u_{Bp}, h_{Rqp}, h_{Bqp}, and f_q indicate the p-directional captured movement of the light gray (red) marker, that of the dark gray (blue) marker, an element of the conversion matrix of the light gray (red) marker, that of the dark gray (blue) marker, and the q-directional applied force, respectively. We obtained f from u by solving the inverse of (1).

It should be noted that GelForce uses a single camera for capturing the movements of the two layers of markers. To calculate the three-dimensional force vector, it is necessary to measure the movements of the markers in a three-dimensional manner. A stereo camera would be suitable but would be too bulky and difficult to calibrate. Hence, to overcome these problems, we used two layers of markers, each of different color, and one camera. The two different colors make is easier to distinguish between the markers. However, the measured marker movements for each layer are not perfectly independent. Therefore, it is difficult to solve the inverse of (1). Thus, we applied the dumped least-squares method [13].

$$\begin{aligned} f &= H^{-g}u \\ H^{-g} &= (H^T H + \omega I)^{-1} H^T u. \end{aligned} \quad (2)$$

In this equation, ω and I represent the dumping factor and unit matrix, respectively.

GelForce does not require any electronic components such as resistors or capacitors. Therefore, it is easy to adapt

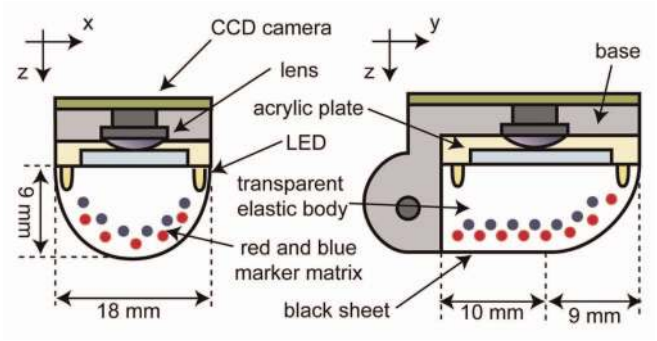

Fig. 3. Configuration diagram of the finger-shaped vision-based haptic sensor.

the shape and size of the GelForce to those of the fingertip. In addition, new developments in camera technology may help us to improve spatial and temporal resolutions of the sensor further. The elastic body of the sensor provides an added advantage. The elasticity enables the sensor to measure haptic information accurately by reproducing the physical interaction involved in the sense of touch. The sensor is also highly durable.

2.2 Design of the Finger-Shaped GelForce

2.2.1 Configuration of the Prototype

Based on the GelForce technology, we constructed a prototype of the finger-shaped GelForce. Ideally, the performance of the sensor should be comparable to that of human beings, as mentioned in chapter 1. However, it was difficult to achieve this performance with current (2008) camera technology. Therefore, we constructed the prototype for the evaluation using a commercially available camera with a video graphics array (VGA) resolution and a frame rate of approximately 60 fps.

The configuration of the prototype is shown in Fig. 3. The transparent elastic body and the CCD camera are attached to the plastic base of the robotic hand. The transparent elastic body is made from silicon rubber (Shin-Etsu Chemical Co., KE-109). Because the conventional GelForce is also made from the same silicon rubber, the linearity of the finger-shaped GelForce appears to be less than 7.5 N [12]. The shape of the elastic body is partly spherical and partly cylindrical; hence, it resembles a human fingertip. The dimensions of its cylindrical and spherical parts are $18 \times 9 \times 10\ \mathrm{mm}^3$ and $18 \times 9 \times 9\ \mathrm{mm}^3$, respectively. The boundary between the elastic body and the base of robotic hand is fixed by a transparent acrylic plate. The camera is custom made comprising a video compression unit and four image-capturing units (ViewPLUS Inc.). The size of the video compression unit and the image-capturing units are $100 \times 100 \times 10\ \mathrm{mm}^3$ and $14 \times 16 \times 1.5\ \mathrm{mm}^3$, respectively. Each image-capturing unit is connected to the video compression unit using a flexible cable. In addition, the video compression unit is connected to a PC using a USB cable. The size of the cable is $20 \times 10 \times 0.5\ \mathrm{mm}^3$. The resolution of each image is 640×480 pixels (VGA). The frame rate of the camera is 67 fps. We used a camera with a wide-angle lens to capture the movements of all the markers. The lens angle of the camera is 110 degree. The diameter and the height of the lens are 14 mm and 6.5 mm, respectively. The constructed prototype and its dimensions

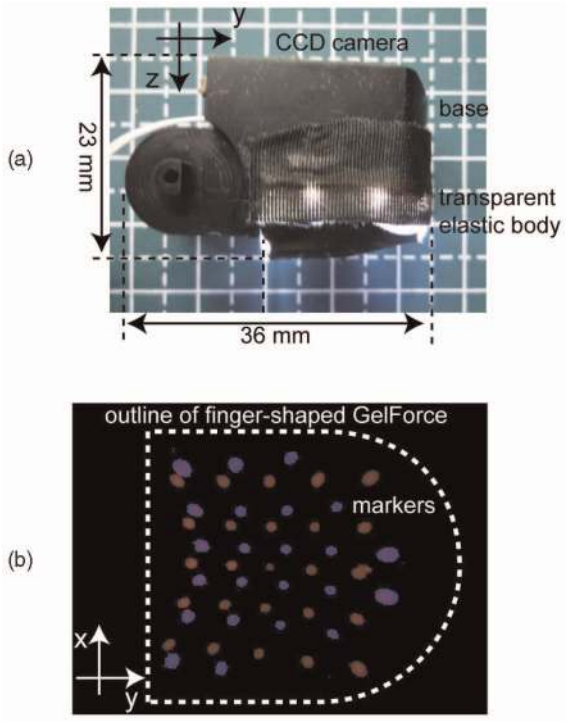

Fig. 4. (a) Constructed prototype of finger-shaped GelForce. This picture was taken from the same view as that of Fig. 3. (b) Captured image of markers by camera. The white dashed line represents the outline of the finger-shaped GelForce from the z-directional view.

are shown in Fig. 4a. The total dimension of the prototype is $18 \times 23 \times 36\ \mathrm{mm}^3$. Fig. 4b shows the images of the markers captured by the camera. To capture the markers clearly, we set their diameters to 0.5 mm (approximately 15 pixels). To prevent the overlapping of the light (red) and dark (blue) gray markers, we also separated them by a distance of 2.5 mm. The light (red) and dark (blue) gray markers were placed at a depth of 0.5 and 2.0 mm, respectively, from the surface of both cylindrical and spherical part. The numbers of light (red) and dark (blue) gray markers are 25 and 23, respectively. We printed the disk markers using a silk-screen printmaking technique. The markers are made from silicon rubber and a colorant. Because the sensor uses vision-based technology, light from the environment produces noise. Therefore, the surface of the sensor is covered with a black sheet made from silicon rubber. In addition, to capture the marker movements clearly, we illuminated them using a light-emitting diode (LED) mounted near the camera. We used eight high-intensity LED chips (audio-Q Inc., AQ-KS1609WC).

2.2.2 Accuracy of Capturing the Marker

The surface traction field is calculated from the movements of the centers of the markers captured by the camera. Therefore, an error that occurs while capturing the movements of the markers may produce noise in the measurement of the force. In this section, we evaluate the accuracy of the measurement of the movements of the markers when no force is applied to the surface of the sensor.

We capture two images of the markers when no force is applied. Then, we displace the markers in one of the images by 5.0 pixels along the x-direction. Displacement vectors of the markers are calculated using these two images. Table 1

TABLE 1
Measurement of Marker Movements

Marker	Direction	Average (pixel)	Standard Deviation (pixel)
Red	+x	4.87	0.14
	+y	0.03	0.14
Bule	+x	4.95	0.13
	+y	0.00	0.10

lists the average and the standard deviations of the x- and y-displacements of the light (red) and dark (blue) gray markers. This result shows that the movements of the markers are measured with subpixel accuracy.

2.3 Conversion Matrix H

2.3.1 The Conventional Analytic Method and Its Disadvantages

In the case of the conventional GelForce, the conversion matrix H in (1) is analytically constructed. On the basis of the assumption that the sensor is a semi-infinite elastic body, we can calculate the elements of H using the elastic theory [14].

Unfortunately, this assumption is not applicable to a finger-shaped GelForce because the shape of this sensor is curved. It may be possible to obtain the conversion equation under a boundary condition that the surface of the elastic body is curved. However, development of a conversion equation is quite difficult.

Another approach to constructing the H involves a planar approximation of the sensor surface. The surface traction field was calculated using elastic theory under the assumption that the curved sensor surface is flat. However, in the finger-shaped GelForce, the movements of markers are captured intricately. Unlike the arrangement of markers in the conventional GelForce, the markers in the finger-shaped GelForce are arranged along the surface, which has a complicated shape. Also, to construct a small sensor, we used a camera with a wide-angle lense. The wide-angle lens distorts the camera image. Therefore, the patterns of the marker movements captured by the camera differ from one marker to the other. The intricacy of marker movements complicates the conversion of marker movements, which is required for satisfying the elastic theory.

2.3.2 Observational Method

Due to the above-mentioned problem, we could not determine H of the finger-shaped GelForce using the analytical method. Therefore, with the finger-shaped GelForce, we estimated the elements of H by observational method. Fig. 5 shows the algorithm used for constructing H. First, we applied forces at each force sampling point and recorded the applied force. Then, we measured the movement of markers. From the recorded forces and measured movement of markers, we estimated H.

Fig. 6 shows the apparatus used for constructing H. The surface of the sensor was pushed using a probe. The edge of the probe is spherical. The probe ideally has a small diameter. However, when we applied a force using the small probe, the probe slipped on the surface of the finger-shaped GelForce. Therefore, we used the acrylic probe with a diameter of both cylindrical and spherical part 5.0 mm. The probe is mounted on a six-axis force sensor (BL NANO, BL Autotech, Ltd.) to measure the magnitude of the applied force. In addition, we used an xyz stage (VSQ-601XYV, Chuo Precision Industrial Co., Ltd.) to control the applied force. The points at which force is applied are shown in Fig. 7. The number of the force sampling points of GelForce depends on the number and density of the markers. In the prototype, the numbers of markers are $25 + 23 = 48$ and they are separated by a distance of 2.5 mm. Therefore, the number of the force sampling points should be less than 32. In this prototype, we applied forces at $5 \times 5 = 25$ points on the surface of the sensor. These points are also separated by a distance of 2.5 mm.

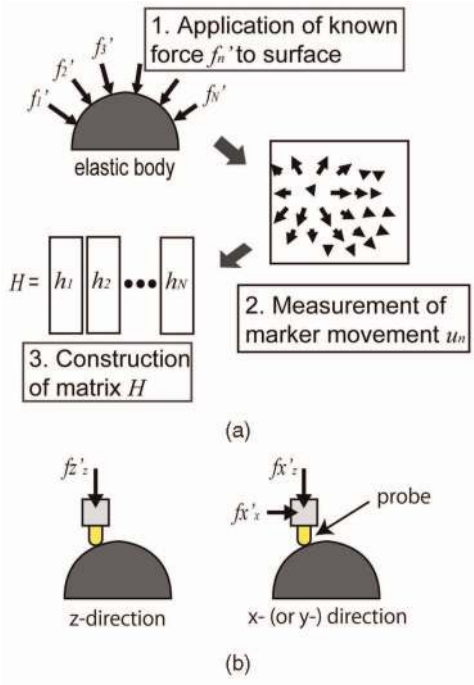

Fig. 5. (a) Algorithm for construction of conversion matrix H. The elements of H are calculated from the measured force f_n' and the movements of the markers denoted by u_n. (b) Application of force to z- and x- (or y-) direction.

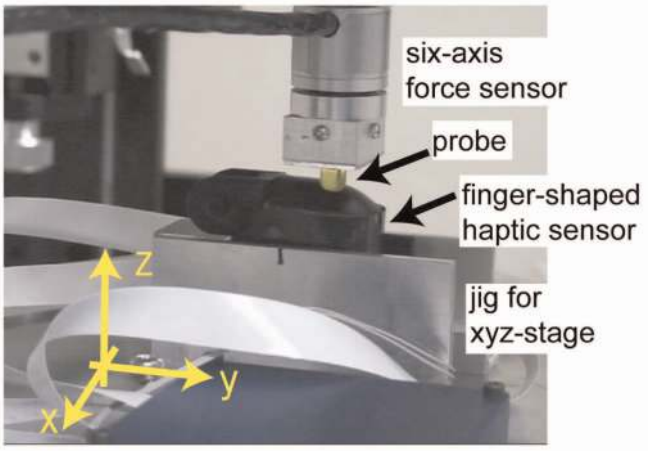

Fig. 6. Image of apparatus used for constructing H.

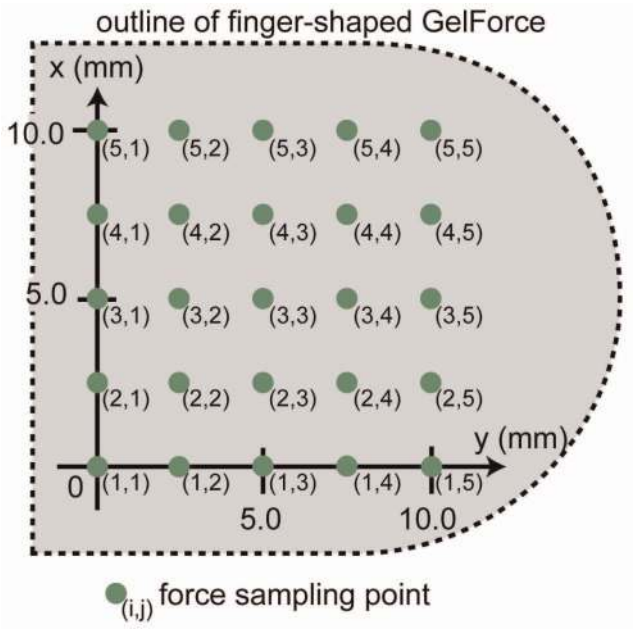

Fig. 7. Force sampling points. (i, j) represents two-dimensional number of sampling points. The black dashed line represents the same outline of the finger-shaped GelForce from the z-directional view illustrated in Fig. 4.

First, forces were applied to the one of the force sampling points along three directions. When we applied a force along the z-direction, the magnitude of the applied force was approximately 1.2 N. It is impossible to apply a force only along the x- or y-direction. Hence, we first applied a force along the z-direction, and then, we applied suitable forces along the x- and y-directions (Fig. 5b). The magnitudes of the applied force along z-direction and x- or y-direction were approximately 1.0 and 0.25 N, respectively. Then, we recorded the force elements resulting from the application of the force by the six-axis force sensor. After applying force along three directions, the recorded forces at the sampling point f'_n were denoted as follows:

$$f'_n = \begin{bmatrix} fx'_x, fy'_x, fz'_x \\ fx'_y, fy'_y, fz'_y \\ fx'_z, fy'_z, fz'_z \end{bmatrix}, \tag{3}$$

where fp'_q is the q-directional element of the force when an p-directional force is applied.

Next, we captured the movements of markers u_n. The movement of this marker is given by (4).

$$u_n = \begin{bmatrix} u_{xx}, u_{yx}, u_{zx} \\ u_{xy}, u_{yy}, u_{zy} \end{bmatrix}, \tag{4}$$

where u_{pq} is the q-directional movement of the marker when the p-directional force is applied. Using f_n and u_n, we can calculate the elements of H at the sampling point as follows:

$$h_n = u_n f'^{-1}_n \left(h = \begin{bmatrix} h_{xx}, h_{yx}, h_{zx} \\ h_{xy}, h_{yy}, h_{zy} \end{bmatrix} \right) \tag{5}$$

In this equation, h_n, u_n, and f'_n represent $2\mathrm{m} \times 3$ conversion matrix, $2\mathrm{m} \times 3$ matrix of m-marker movements, and 3×3 matrix of a force, respectively. Using this equation at N-force sampling points (in this prototype, $\mathrm{N} = 25$), we can construct H by (6).

$$H = [h_1, h_2, \ldots, h_n, \ldots, h_N]. \tag{6}$$

When we calculate the H^{-g} from the constructed H, the damping factor causes some errors to the H^{-g} in (2) [13]. Therefore, to calibrate the finger-shaped GelForce, we determined a constant that fits the magnitude of the force calculated using the finger-shaped GelForce to that of the force measured using the six-axis force sensor.

3 Evaluation of Sensor Performance

In this section, we evaluate the basic performance of the constructed prototype. We evaluate the following three criteria: force magnitude, spatial resolution, and the time required for carrying out various calculations such as evaluation of the conventional GelForce [12]. By drawing a comparison between the performance of the finger-shaped GelForce and that of the conventional GelForce, we examine the validity of the observationally constructed H. The apparatus used for evaluating the environment is the same as that used for constructing H (Fig. 5).

3.1 Magnitude

We evaluate the linearity, resolution, and independency of the magnitude of the applied force along the following three directions: x, y, and z. Because of the small size of the finger-shaped GelForce, the linearity of its elastic body seems not to be assumed when a large force is applied. Therefore, first, we evaluate the linearity of the sensor along z-direction. Then, we evaluate the resolution and independency of the magnitude of the force along the above-mentioned three directions.

While evaluating the magnitude of the applied force, we draw a comparison between the measured force vectors F and the applied force F'. The applied force F' is measured using the six-axis force sensor and the controlled xyz stage. Force is applied at the center of the surface of the sensor, where $\mathrm{x} = 5.0$ mm and $\mathrm{y} = 5.0$ mm, as shown in Fig. 7. In this evaluation, we applied a force using a cylindrical probe with a diameter of 10 mm. When a finger touches an object, the contact area is usually a surface, and not a point. Therefore, we used a wide probe to evaluate the performance of the sensor in a manner similar to an actual contact. Furthermore, the measured force from GelForce should be evaluated by the total of force at every sampling point because independency of each sampling point is not confirmed. Therefore, each directional force, denoted by F_x, F_y, and F_z, is calculated using (7).

$$\begin{aligned} F_x &= \sum_{i,j}^{5,5} fx_{ij}, \\ F_y &= \sum_{i,j}^{5,5} fy_{ij,} \\ F_z &= \sum_{i,j}^{5,5} fz_{ij}. \end{aligned} \tag{7}$$

In this equation, i and j are the numbers of the force sampling point in Fig. 7, fx_{ij}, fy_{ij}, and fz_{ij} are represented as one-dimensional force vectors along each direction.

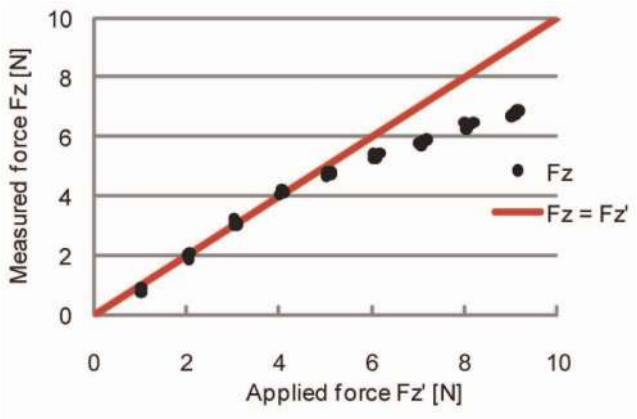

Fig. 8. Evaluation of linearity of the finger-shaped GelForce in z-direction.

3.1.1 Preliminary Experiment of Linearity

While evaluating linearity, we applied an increasing force and investigated the limitation of linearity. Because of the complicated shape of the sensor, it is difficult to apply a large force along the x- or y-direction. Therefore, we evaluate the linearity of the magnitude only along the z-direction.

We applied a force of 1.0-10.0 N along the z-direction by increasing its magnitude in steps of 1.0 N. Values of the z-directional force obtained by using the finger-shaped GelForce and six-axis force sensor are recorded. The measurement procedure is repeated five times.

Graph shown in Fig. 8 presents the results of evaluation. The horizontal and vertical axes represent the applied force and the measured force, respectively. The dots show the results of each trial. The line shows that the applied force is equal to the measured force. From these results, it is observed that the linearity of the magnitude is below 4.0 N.

3.1.2 Resolution, Independency, and Linearity

While evaluating resolution and independency, we investigated the measurement accuracy of the magnitude and direction of the force along the three directions. In the evaluation of the conventional GelForce, resolution of magnitude along the z-direction and the resolution of angle are examined. In addition, it is also essential to examine the resolution of the magnitude and the coupling effect of the sensor along the three directions. It is found that due to the complicated shape of the sensor, measurement noise is generated along the x- or y-direction. Therefore, in the case of the finger-shaped GelForce, we examine the resolution of magnitude instead of the resolution of angle along the x- and y-directions.

To investigate the resolution of magnitude along the x- and y-directions, we first applied a force of 2.0 N along the z-direction. Then, we applied the force of 0.2-2.0 N along the x- or y-direction by increasing its magnitude in steps of 0.2 N. To investigate the resolution of magnitude along the z-direction, we applied a force of 0.2-2.0 N along the z-direction by increasing its magnitude in steps of 0.2 N. From Fig. 8, it can be observed that the finger-shaped GelForce seems to be linear under these applied forces. The force values obtained using the finger-shaped GelForce and six-axis force sensor is recorded. We recorded all the directional forces applied for each

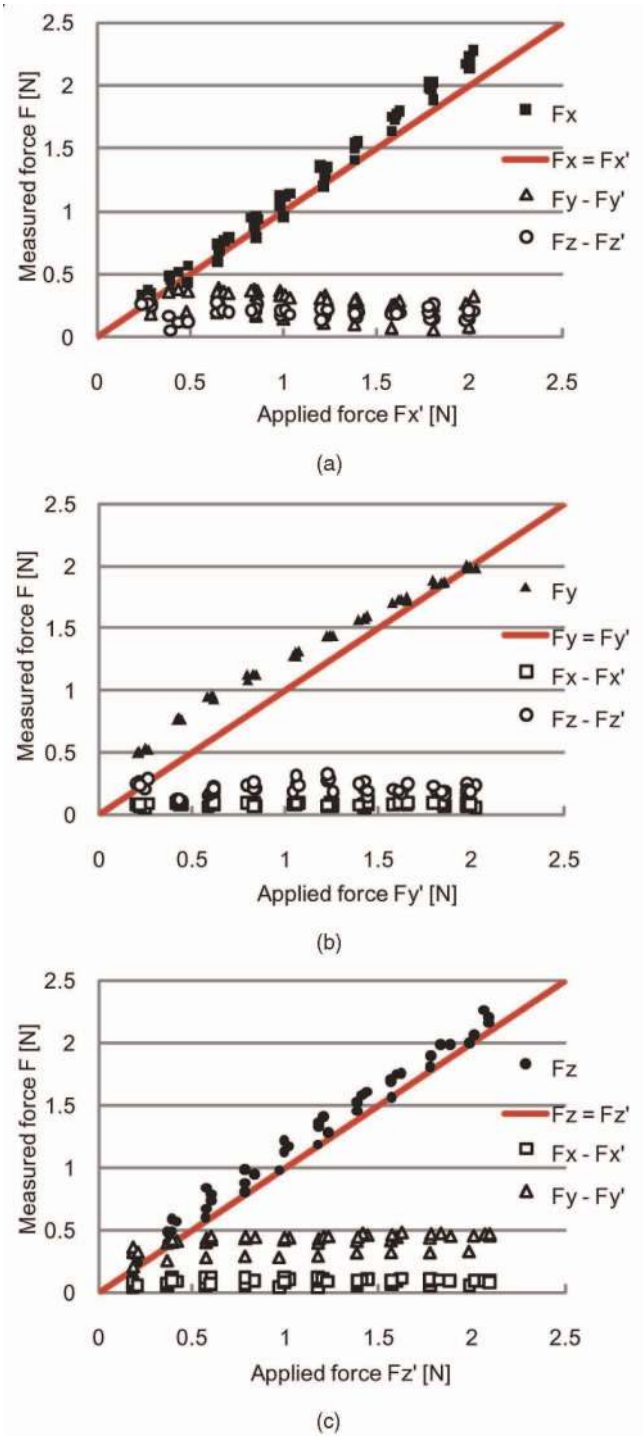

Fig. 9. Relationship between the applied force and measured force along the (a) x-direction, (b) y-direction, and (c) z-direction.

experiment. The measurement procedure is repeated five times for each direction.

Graphs shown in Fig. 9 present the results of evaluation. The horizontal and vertical axes represent the applied force and the measured force, respectively. The black squares, triangles, and dots represent the absolute value of F_x, F_y, and F_z, respectively. Each outline dots represent coupling effects in each direction. To clearly show the measured force in each graph, we compensated the values of directional forces other than the force applied direction. For example,

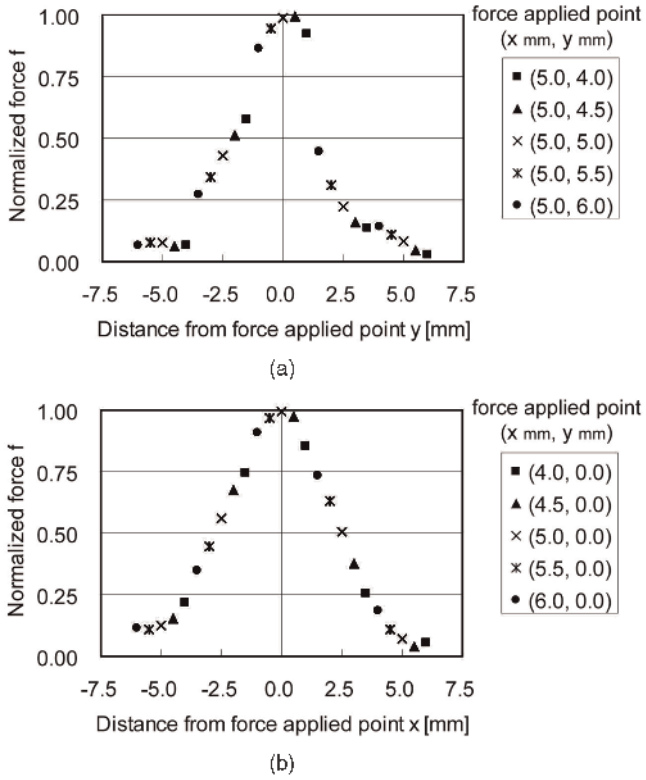

Fig. 10. Force measured by high-density sampling. (a) and (b) graphs show the results of applying a force at the center and edge of the sensor, respectively.

when we applied an x-directional force, we subtracted the y- and z-directional applied forces F'_y and F'_z from F_y and F_z, respectively. The line in this graph shows that the applied force is equal to the measured force. From these results, it is observed that the maximum resolution of the magnitude of the force is 0.3 N along each direction. The magnitude of the other directional elements of the force is approximately below 0.3 N, other than y-directional element of graph (c); 0.5 N.

3.2 Spatial Resolution

In this section, we evaluate the spatial resolution of the sensor. To carry out this evaluation, we determine the magnitude of each force vector when a force is applied at a certain point on the surface of the elastic body. The magnitude of the force vector f_{ij} is calculated using (8).

$$f_{ij} = \sqrt{fx_{ij}^2 + fy_{ij}^2 + fz_{ij}^2}. \quad (8)$$

It should be noted that the sampling interval is too large to evaluate the spatial resolution. Therefore, we adopt the following procedure to evaluate the spatial resolution. Two adjacent sampling points on the surface of the sensor are selected. The distance between these two points is subdivided into n points, and a known force is applied along the z-direction at each point. Then, the force vectors at each point are calculated by considering each point as the origin. A graph is constructed by plotting the distance from each origin and the calculated force magnitude on the horizontal and vertical axes, respectively. By using the method explained above, the density of the points in the sampling region increases. The spatial resolution of the force distribution can be obtained from the slope of the graph.

TABLE 2
Calculation Time

Number of Sensor Units	Average [μs]	Std. Deviation [μs]
1	545	56
4	2159	43

The magnitude of the force applied along the z-direction is fixed at 2.0 N. The diameter of the spherical probe that is used to apply the force is 5.0 mm. In this condition, the displacement of the probe into the skin is approximately 1.3 mm. Adjacent sampling points are located at the center and edge of the area in which the force field is measured. The actual sampling interval is 2.5 mm, and the distance between adjacent points is subdivided into intervals of 0.5 mm. In the case of the conventional GelForce, the spatial resolution is examined only at the center of the sensor. However, in the case of the finger-shaped GelForce, the shape of the sensor influences its spatial resolution. Therefore, we evaluate the spatial resolution at both the center ($\mathrm{x} = 5.0$ mm and $\mathrm{y} = 5.0$ mm in Fig. 7) and the edges ($\mathrm{x} = 5.0$ mm and $\mathrm{y} = 0.0$ mm, $\mathrm{x} = 0.0$ mm and $\mathrm{y} = 5.0$ mm in Fig. 7) of the surface of the sensor and along both the x- and y-directions.

We obtained approximately the same results for all measurement points and directions. Fig. 10 shows the representative results of the experiment. The first graph shows the results obtained by applying a force at the center of the sensor. The second graph shows the results obtained by applying a force at the edge of the sensor. The values plotted on the vertical axis are normalized using the maximum value of the force magnitude. The dots in the graphs represent the points at which the force is applied (x [mm], y [mm] in Fig. 7).

From the graphs shown in Fig. 10, it can be observed that the full width half maximum is approximately 5.0 mm. Therefore, the spatial resolution of the force is estimated to be approximately 5.0 mm. These results are identical to those obtained by carrying out evaluations at other points and directions.

3.3 Time

To perform a dexterous operation, we need to obtain haptic information from multiple sensors. Therefore, we must process a large amount of information obtained from different sensors simultaneously. In this section, we evaluate the calculation times of the single finger-shaped GelForce and four sensor units.

Calculation time is obtained from the frequency of the CPU. In this experiment, the speed of the processor used in the PC is 2.8 GHz (Intel PentiumD processor). The program runs on Windows XP SP2. The accuracy of measurement is 1 μs. The calculation time is measured over 100 trials, and the average and standard deviation of the calculation time are listed in Table 2. The sensor units represent the finger-shaped GelForce attached to the video compression unit.

In this prototype, the camera unit captures four images at 67 fps. Therefore, the PC must calculate the surface

TABLE 3
Performance of Conventional and Finger-Shaped GelForce

Feature	Conventional [12]	Finger-shaped
Size of elastic body	100 × 100 × 40 mm³	16 × 16 × 10 mm³
Marker interval	3 mm	2.5 mm
Camera	VGA, 30 fps	VGA, 67 fps
Linearity (z-direction)	<7.5N	<4.0N
Resolution of magnitude	0.3 N	0.3 N
Resolution of angle	5°	(6°)
Spatial resolution	4 mm	5 mm
Refresh rate	30 Hz	67 Hz

Value shown in parentheses is the estimated one.

traction fields of the four sensors within 14 ms. The result of this experiment satisfies this requirement even when we process information obtained from the four sensor units simultaneously.

3.4 Discussion

We compared the performance of the finger-shaped GelForce with that of the conventional GelForce; the results of this comparison are summarized in Table 3. Because of the small size of the finger-shaped GelForce, it is confirmed the linearity of force is below 4.0 N. However, Fig. 8 shows a one-to-one relationship between the applied and measured forces. Therefore, we can measure a force rather than 4.0 N by compensating for the nonlinearity of the sensor.

The resolution of magnitude of the finger-shaped GelForce is same as that of the conventional GelForce. However, Fig. 9b shows an offset in the y-directional force, and Fig. 9c shows a y-directional element of approximately 0.5 N. We consider that the shape of the sensor is responsible for the formation of an unintended directional element of force. We also consider that the shape of the sensor is responsible for the nonlinearity of the x- or y-directional force greater than 1.0 N. The coupling effect of the sensor is small in all directions. Furthermore, when we estimate the resolutions of angle from the results of Figs. 9a and b, the resolution is approximately 6 degree. Therefore, the three directional force vectors seem to be calculated correctly. Furthermore, because the magnitude resolution is depend on the camera resolution in GelForce, we can expect further improvement of the resolution and archive 0.5 mN [3] in the future.

The spatial resolution of the finger-shaped GelForce is lower than that of the conventional GelForce. However, in this prototype, we construct the conversion matrix in 2.5 mm force sampling interval. From the sampling theory, 5.0 mm spatial resolution is reasonable. The spatial resolution is expected to improve with an increase in the density of the sampling points and markers. For example, in the case of the sensor, to obtain a spatial resolution similar to that of the human fingertip (approximately 1.2-1.7 mm [4]), the distance of force sampling point should be under 0.9 mm. To archive this value, the distance between the markers and the diameter of each marker should be approximately 0.2 mm and 0.9 mm, respectively. In the prototype, the diameter of the marker is 0.5 mm or 10-20 pixels, and the error in the measurement of the marker movement is 0.15 pixels. Therefore, we can reduce the size of the markers and the distance between them in order to meet the desired specifications. Furthermore, we can expect a further improvement in the spatial resolution with an increase in the camera resolution. The discontinuous result shown in Fig. 10a is considered to be obtained due to an error in the calculation of the pseudoinverse matrix using (2).

Time resolution of the sensor can also be improved. When we consider the human performance of haptic perception, it is required to maintain the refresh rate of the force sensor to greater than 700 Hz [5]. In the case of the prototype sensor, the calculation time is small, i.e., less than 2.5 ms even after using four sensors. Therefore, a time resolution of 700 Hz can be easily archived by improving the performance of the computer and frame rate of the camera.

From these results, we consider that the finger-shaped GelForce can be used to measure surface traction fields using the observationally constructed conversion matrix. Therefore, we believe that the implementation of this haptic sensor will enable robotic hands to perform dexterous operations.

4 Field Test

We developed a finger-shaped GelForce as a haptic sensor for a robotic hand. In this section, we have discussed the implementation of the finger-shaped GelForce for use in a conventional robotic hand and performed a grasping of an object as a field test.

Through the grasping operation, we have illustrated an operation that is performed using the haptic information acquired by the finger-shaped GelForce. Furthermore, we have shown that the finger-shaped GelForce can be used to correctly measure the surface traction field in actual use. When we implement the finger-shaped GelForce for the robotic hand, the vibration and movement of the robotic finger can prevent the accurate measurement of the surface traction fields. Therefore, we have evaluated those surface traction fields that were measured during the grasping operation performed by the robotic hand.

4.1 Implementation to Robotic Hand

We use a multifingered robotic hand [15] as a humanoid robotic hand. Fig. 11 shows a robotic hand with the finger-shaped GelForce. This hand has a total of 15 degrees of freedom (DOFs)—five DOFs for the thumb, one for abduction of other fingers, three for the index finger, and two each for the remaining fingers. Each fingertip also has an independent DOF. The thumb has a number of DOFs, which enables to cover wide range of movements of the thumb. In addition, this DOF allows the index finger and the thumb to be countered.

The control unit is placed on the back of the hand. This unit is connected to the PC through a Controller Area Network (CAN) interface card (CBI4852, Interface Corp.). We control the robotic hand by using a PID control at 1 kHz. However, time resolution of the finger-shaped GelForce is approximately 67 Hz. This large calculation time causes instability and hampers the control of the robotic hand. Therefore, we use two PCs, i.e., one for controlling the robotic hand, and the other for calculating the finger-shaped GelForce. We connect both these PCs through LAN and transmit haptic information at 67 Hz using a UDP.

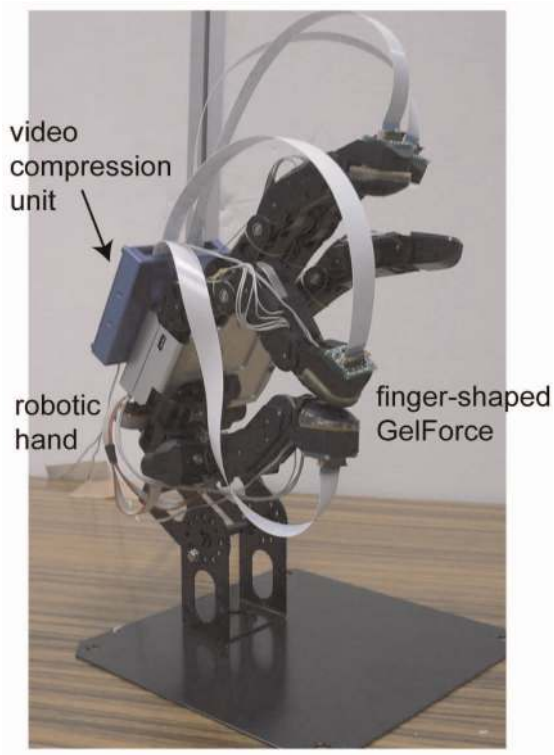

Fig. 11. Robotic hand with finger-shaped GelForce.

We attach four finger-shaped GelForces at the fingertips of the thumb, index finger, middle finger, and annular finger of the robotic hand. Properties of the finger-shaped GelForce are the same as those of the constructed prototype discussed in chapter 2. The video compression unit is placed on the back of the robotic hand.

4.2 Grasping Operation

In order to perform a field test on the finger-shaped GelForce, we performed simple grasping operations using the robotic hand. Ideally, the operation using the measured surface traction field is desired. However, because the surface traction field contains much information, it is difficult to clearly show the efficiency of surface traction field. Therefore, we shrunk the surface traction field and conducted two operations. One operation involved the control of the grasping force using the three-dimensional force. In this evaluation, we used the finger-shaped GelForce as a *force vector sensor*. The other operation involved the control of the grasping position using the center of the force vector distribution. In this evaluation, we used the singer-shaped GelForce as a *force distribution sensor*.

4.2.1 Control of Grasping Force

The measurement and control of the grasping force avoids the application of a considerable force to an object. This control enables soft grasping so as not to damage the object and the robotic hand. Furthermore, the measurement of a frictional force and an increase in the grasping force prevent the dropping of the object. Therefore, controlling the grasping force using the three-dimensional force information is important in order to ensure the safety and stable grasping of the object.

In the operation that involves the control of the grasping force, the robotic hand grasps a styrofoam ball between the thumb and the index finger, as shown in Fig. 12. The diameter and weight of the ball are 60 mm and 5.7 g, respectively. To grasp the ball, we apply a torque to rotate the index finger and thumb about the x-axis. The grasping force is controlled at an arbitrary value to ensure that the ball does not move. When we apply a force to the ball along the x-direction, the finger-shaped GelForce detects the frictional force and increases the grasping force of the fingers. The applied force is approximately 0-1.5 N. The additional grasping force is proportional to the frictional force. The proportionality constant is determined by performing a preliminary experiment whose objective is to ensure that the grasped ball is not dropped. When the grasping force exceeds 4.0 N, the torque of the thumb is set to zero. We have measured the grasping force F_z and the frictional force F_x of the thumb using (7). In addition, we have measured the torque T_x that rotates the base of the thumb about the x-axis.

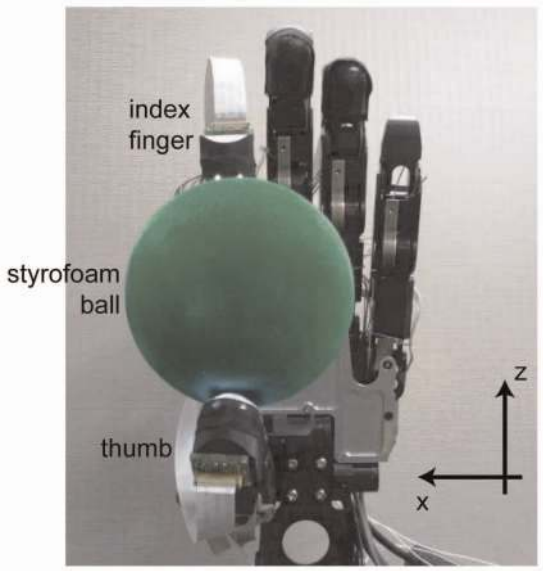

Fig. 12. Setup for controlling robotic hand. Robotic hand grasps a Styrofoam ball by its index finger and thumb. Thumb moves along the x- or z-direction in each experimental operation.

The results of the abovementioned experiment are shown in Fig. 13. In this figure, the horizontal and vertical axes represent the operation time and the measured value,

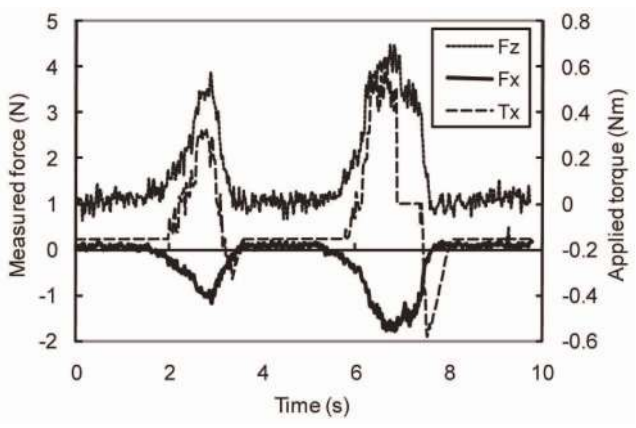

Fig. 13. Result of controlling grasping force. *Fz*, *Fx*, and *Tx* represent grasping force, frictional force, and torque of thumb, respectively.

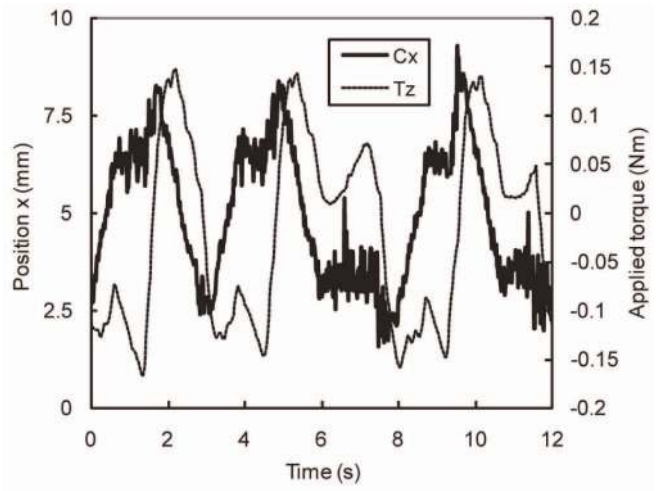

Fig. 14. Result of controlling grasping position. *Cx* and *Tz* represent the grasping position and torque of thumb, respectively.

respectively. This figure shows that F_x increase with the applied force. Furthermore, F_z and T_x increase in proportion to F_x. During this operation, the ball did not move. Therefore, we confirmed that the force vector was measured correctly enough to control the grasping force.

4.2.2 Control of Grasping Position

When a robotic hand grasps an object, attention must be paid to the grasping position on its fingertip. Recognition of the grasping position enables the robotic hand to control the object dexterously.

In the operation that involves the control of the grasping position, the robotic hand grasps the same styrofoam ball as that used before, as shown in Fig. 12. Then, the robotic hand rotates its thumb about the z-axis such that the thumb alternately moves to the right and then to the left along the x-direction. During this movement, the finger-shaped GelForce measures the grasping position C (C_x, C_y) of the ball on the thumb. Using (9), C (C_x, C_y) is calculated to be the center of the size of the force vectors.

$$\begin{pmatrix} C_x \\ C_y \end{pmatrix} = \frac{1}{S}\sum_{i,j}^{5,5} f_{ij}\begin{pmatrix} i \\ j \end{pmatrix}, \qquad S = \sum_{i,j}^{5,5} f_{ij}. \tag{9}$$

In this equation, i and j are the numbers of the force sampling point in Fig. 7, and f_{ij} is the size of the force vector calculated using (8). When the grasping position C_x exceeds 7.5 mm or is below 2.5 mm, the direction of rotation of the thumb is inverted. We measure the grasping position c_x and the torque T_z that is responsible for rotating the thumb.

The results of the abovementioned experiment are shown in Fig. 14. In this figure, the horizontal and vertical axes represent operation time and measured value, respectively. When C_x exceeds 7.5 mm or falls below 2.5 mm, T_z is inverted to move the thumb in the counter direction. This control ensures that the grasping position is maintained around the center of the thumb, i.e., at 5.0 mm. Therefore, we confirmed that the grasping position is correctly measured and used for controlling the robotic hand.

4.3 Discussion

From the above two examples of grasping operations, we confirmed that the finger-shaped GelForce can be used in practice. In these simple operations, we used the finger-shaped GelForce as a *force vector sensor* or *force distribution sensor*. We reduced the surface traction fields to the three-dimensional force at a point or the center of the force vectors. Therefore, these two experiments do not show the full performance of the developed sensor. We believe that it is possible to perform more complicated operations by combining this reduced surface traction field or directly using the surface traction fields. It is a future work to design and conduct an experiment in order to show the full performance of the developed sensor

5 Conclusion

We developed a finger-shaped GelForce as a haptic sensor for a robotic hand that can be used to measure surface traction fields. This sensor was developed on the basis of technology used in the vision-based haptic sensor GelForce. Because of the complicated shape of the finger-shaped sensor, we proposed an observational method in order to develop a prototype of the sensor. Then, we evaluated the basic performance of the sensor and conducted a field test using a robotic hand. The results of the evaluation show that the finger-shaped GelForce is applicable to the robotic hand.

The finger-shaped GelForce is a vision-based surface traction field sensor that has a simple structure and processing method. Therefore, the performance of the sensor can be easily improved using a high quality camera. We believe that a humanoid robot with the finger-shaped GelForce will be able to perform dexterous operations in our daily life.

Acknowledgments

This work had technical support on development of the finger-shaped GelForce from Nitta Corporation, and work was partially supported by a grant from the Ministry of Internal Affairs and Communications SCOPE and Grant-in-Aid for JSPS Fellows (20·10009).

References

[1] H.R. Nicholls and M.H. Lee, "A Survey of Robot Tactile Sensing Technology," *Int'l J. Robotics Research*, vol. 8, pp. 3-30, 1989.
[2] M.H. Lee and H.R. Nicholls, "Tactile Sensing for Mechatronics—A State of the Art Survey," *Mechatronics*, vol. 9, pp. 1-31, 1999.
[3] R.S. Johansson, A.B. Vallbo, and G. Westling, "Theresholds of Mechanosensitive Afferents in the Human Hand as Measured with von Frey Hairs," *Brain Research*, vol. 184, pp. 343-351, 1980.
[4] F. Bega-Bermudez and K.O. Johnson, "Differences in Spatial Acuity between Digits," *Neurology*, vol. 56, pp. 1389-1391, 2001.
[5] R.T. Verrillo, "Effect of Contactor Area on Vibrotactile Threshold," *J. Acoustical Soc. of Am.*, vol. 35, pp. 1962-1966, 1963.
[6] R.S. Fearing, "Using a Cylindrical Tactile Sensor for Determining Curvature," *IEEE Trans. Robotics and Automation*, vol. 7, no. 6, pp. 806-817, Dec. 1991.
[7] J.G. Silva, A.A. Carvalho, and D.D. Silva, "A Strain Gauge Tactile Sensor for Finger-Mounted Applications," *IEEE Trans. Instrumentation and Measurement*, vol. 51, no. 1, pp. 18-22, Feb. 1991.

[8] D.T. Pawluk, J.S. Son, P.S. Wellman, W.J. Peine, and R.D. Howe, "A Distributed Pressure Sensor for Biomechanical Measurements," *J. Biomechanical Eng.,* vol. 120, no. 2, pp. 302-305, 1998.
[9] M. Ohoka, Y. Mituya, K. Hattori, and I. Higashioka, "Data Conversion Capability of Optical Tactile Sensor Featuring an Array of Pyramidal Projections," *Proc. IEEE Int'l Conf. Multisensor Fusion and Integration for Intelligent Systems,* pp. 573-580, 1996.
[10] N.J. Ferrier and R.W. Brockett, "Reconstructing the Shape of a Deformable Membrane from ImageData," *The Int'l J. Robotics Research,* vol. 19, no. 9, pp. 795-816, 2000.
[11] S. Saga, H. Kajimoto, and S. Tachi, "High-Resolution Tactile Sensor Using the Deformation of a Reflection Image," *Sensor Rev.,* vol. 27, pp. 35-42, 2006.
[12] K. Kamiyama, K. Vlack, T. Mizota, H. Kajimoto, N. Kawakami, and S. Tachi, "Vision-Based Sensor for Real-Time Measuring of Surface Traction Fields," *IEEE Computer Graphics and Applications Magazine,* vol. 25, no. 1, pp. 68-7, Jan. 2005.
[13] W. Menke, *Geophysical Data Analysis: Discrete Inverse Theory.* Academic Press Inc., 1989.
[14] L.D. Landau and E.M. Lifshitz, *Theory of Elasticity.* Butterworth Heinemann, 1985.
[15] K. Hoshino and Y. Kawabuchi, "Pinching at Finger Tips for Humanoid Robot Hand," *J. Robotics and Mechatronics,* vol. 17, no. 6, pp. 655-663, 2005.

Katsunari Sato received the BS degree in engineering from Tohoku University in 2006, and the MS degree in information Science and Technology from the University of Tokyo in 2008. He has been working toward the PhD degree at the Graduate School of Information Science and technology, and a JSPS research fellow for young scientists since 2008. His research interests include haptic interfaces for telexistence. He received the Dean's Award from IST, the University of Tokyo, in 2008. He is a student member of the IEEE.

Kazuto Kamiyama received the BS, MS, and PhD degrees in Information Science and Technology from the University of Tokyo in 2001, 2003, and 2006, respectively. From 2006 to 2009, he was an assistant professor at the University of Tokyo. He is currently an assistant professor at the University of Electro Communications. His research interests include tactile sensors and virtual reality.

Naoki Kawakami received the MS degree in engineering from Tokyo Institute of Technology in 1996, and the PhD degree in advanced interdisciplinary studies from the University of Tokyo in 1999. He was an assistant professor and a lecturer in the Department of Information Physics and Computing at the University of Tokyo from 1999 to 2002 and from 2002 to 2009, respectively. His research interest is virtual reality.

Susumu Tachi received the BE, MS, and PhD degrees in mathematical engineering and information physics from the University of Tokyo in 1968, 1970, and 1973, respectively. He joined the Faculty of Engineering at the University of Tokyo in 1973, and in 1975, he moved to the Mechanical Engineering Laboratory, Ministry of International Trade and Industry, where he served as the director of the Biorobotics Division. In 1989, he rejoined the University of Tokyo and was a professor in the Department of Information Physics and Computing until March 2009. He is currently a professor emeritus at the University of Tokyo and a professor of Graduate School of Media Design at Keio University. From 1979 to 1980, he was a Japanese Government Award Senior Visiting Scientist at the Massachusetts Institute of Technology, Cambridge. His present research covers robotics, virtual reality and augmented reality with special focus on telexistence (TELESAR and TWISTER), Real-time Remote Robotics (R-Cubed), and Retroreflective Projection Technology (RPT), including optical camouflage. He is a founding director and a fellow of the Robotics Society of Japan (RSJ), the 46th president and a fellow of the Society of Instrument and Control Engineers (SICE), a fellow of the Japan Society of Mechanical Engineers (JSME), and is the founding president of the Virtual Reality Society of Japan (VRSJ). From 1988, he serves as Chairman of the IMEKO (International Measurement Confederation) Technical Committee 17 on Measurement in Robotics. He initiated and founded ICAT (International Conference on Artificial Reality and Telexistence) in 1991 and IVRC (International-Collegiate Virtual Reality Contest) in 1993. He is a member of the IEEE VR Steering Committee and served as general chair of the IEEE VR 2001 and 2002. He is a member of the IEEE.